JOURNAL OF COMPUTATIONAL PHYSICS 53, 42–71 (1984)

Steady-State Solutions of the Euler Equations in Two Dimensions: Rotating and Translating *V*-States with Limiting Cases. I. Numerical Algorithms and Results*

H. M. WU,† E. A. OVERMAN II, AND N. J. ZABUSKY

Institute for Computational Mathematics and Applications, Department of Mathematics and Statistics, University of Pittsburgh, Pittsburgh, Pennsylvania 15261

Received August 10, 1982; revised May 17, 1983

New second- and third-order algorithms are presented for calculating translating and rotating steady-state solutions of the 2D incompressible Euler equations (which we call *V*-states). These are piecewise constant regions of vorticity and the contours bounding them are obtained by solving iteratively a nonlinear integro-differential equation. New *limiting* contours with *corners* are obtained and compared with local analytical solutions. The precise results correct mistakes for limiting contours that were previously given.

1. INTRODUCTION

Solutions of the two-dimensional incompressible Euler equations will elucidate properties of very large Reynold's number flows, as may occur in planetary atmospheres and oceans. The method of contour dynamics, introduced by Zabusky *et al.* [1], provides a computationally convenient approach because a two-dimensional problem is reduced to one dimension. That is, in contour dynamics the sources of the flow are piecewise-constant regions of vorticity, which we call FAVRs (finite area vortex regions) or, equivalently, the contours bounding these regions.

The parameters that describe the range of existence and stability of steady-state FAVR configurations may elucidate properties of these flows. Kirchoff [2] found that an elliptical FAVR was a steady-state solution and Love [3] investigated its stability. No other closed form solutions have been found. Deem and Zabusky [4] found new steady-state FAVR configurations by solving numerically a nonlinear integro-differential equation for the contours using a Newton–Raphson procedure. For example, they found several isolated rotating states of m-fold symmetry that are bifurcations from harmonic waves on a circular FAVR and one isolated symmetrically

* Technical Report ICMA-82-44.

† Permanent address: Computer Center, Academia Sinica, Beijing, China.

0021-9991/84 $3.00

shaped dipolar (i.e., oppositely signed vorticity) translating state. Examples are sketched in Fig. 1. They considered these regions of piecewise-constant vorticity as members of larger sets of steady-state solutions and referred to them generic ly as "V-states." Saffman and colleagues also applied this technique to calculate shapes of doubly connected rotating V-states [5] and periodic states modeling free shear layers [6] and wakes [7]. Pierrehumbert [8] applied an efficient first-order relaxation method and obtained twelve members of the set of symmetrically shaped dipolar translating states. Pierrehumbert and Widnall [9] also applied this algorithm to calculate free shear layer models. Burbea and Landau [10] applied the same algorithm and obtained further examples of m-fold symmetric rotating V-states for $3 \leqslant m \leqslant 6$. In both [8] and [10] the *limiting* V-states, where the contour is nonanalytic, are defective. This occurs because their algorithms seem unable to handle singular and near-singular contours and because the spatial resolution is inadequate in regions of large curvature. In the latter paper, this results in errors in the numerical calculation of the parameter range of existence of rotating V-states. The analytical calculation by Burbea [11] of this range is also incorrect and both calculations are discussed in Section 6.

In this paper we present a new, fast, accurate and computationally efficient algorithm which requires about the same number of iterations to converge as those described above and is capable of treating the limiting V-states. Our numerical results are compared with a local analysis in the neighborhood of nonanalyticity. For the translating V-state, there are two possible limiting cases: the two regions may touch at one point or they may have a common boundary. Analytically, we have been able to exclude the former case. For the latter case we have established analytically that the two (one-sided) tangent angles at a nonanalytical point may *differ* only by $\pi/2$ (i.e., a corner). Numerically, we have confirmed the existence of this solution as shown in Fig. 4b. For the rotating V-states we have established analytically that the tangent angles at a nonanalytical point may *differ* only by 0 (i.e., the tangent angle is continuous) or $\pi/2$. Numerically, we have confirmed the existence of the $\pi/2$ corner for $3 \leqslant m \leqslant 6$ as shown in Fig. 7.

In a recent letter, Saffman and Tanveer [12] also did a local analysis of the limiting translating case and obtained a $\pi/2$ corner. They also used numerical methods to calculate this state, but only provide a gross figure and insufficient information to allow a detailed comparison of results.

In Section 2 we present analytical preliminaries and derive two nonlinear integro-differential equations for the boundary which are the basis for our new second- and third-order accurate algorithms. In Section 3 we analyze the limiting cases in regions where a contour may become nonanalytical and prove the claims made above. In Section 4 we present the discretized versions of the integro-differential equations and iterative algorithms for obtaining both translating and rotating V-states. In Sections 5 and 6 we discuss properties of the numerical solutions for translating and rotating V-states, respectively. In both cases, magnified views of the contours are given in the region of nonanalytical behavior and they are compared to the local solutions of Section 3. We also present a thorough discussion of the sensitivity of the results in the

neighborhood of nonanalytical points to algorithms, discretization procedures, error criteria, and boundary conditions.

2. The Integro-Differential Equations for V-States

The Euler equations can be written in vorticity-stream function form as

$$\omega_t + u\omega_x + v\omega_y = 0, \tag{2.1a}$$

where

$$\Delta\psi = -\omega, \tag{2.1b}$$

and

$$(u, v) \equiv (\psi_y, -\psi_x). \tag{2.1c}$$

If the vorticity is represented by a set of N_c piecewise constant functions of strength ω_j in regions D_j with boundaries ∂D_j, we can express the stream function as

$$\psi(x, y) = \sum_{j=1}^{N_c} \omega_j \iint_{D_j} G(x - \xi, y - \eta)\, d\xi\, d\eta, \tag{2.2}$$

where G is the Green's function for the Laplacian in the unbounded domain

$$G(x - \xi, y - \eta) = -(2\pi)^{-1} \log[(x - \xi)^2 + (y - \eta)^2]^{1/2} = -(2\pi)^{-1} \log l. \tag{2.3}$$

If Green's theorem is applied to the result of substituting (2.2) into (2.1c) we obtain an expression for the velocity as a sum over the N_c contour integrals, namely,

$$(u, v) \equiv (u(x, y), v(x, y)) = (2\pi)^{-1} \sum_{j=1}^{N_c} [\omega]_j \int_{\partial D_j} \log l(d\xi, d\eta), \tag{2.4}$$

where $[\omega]_j$ is the jump in vorticity (outside–inside) at ∂D_j and where the dependence on time has been suppressed. If we integrate by parts we obtain

$$(u, v) = (2\pi)^{-1} \sum_{j=1}^{N_c} [\omega]_j \int_{\partial D_j} l^{-1}(x - \xi, y - \eta)\, dl. \tag{2.5}$$

The contours are assumed to be piecewise Liapunov, where a Liapunov curve is one which possesses a unique continuous *tangent angle*, α, but not necessarily a curvature, at each point [13, 14]. Thus, we require that each contour consists of a finite number of segments, each of which possess a unique α at every point but may have an infinite curvature at the ends.

Kelvin's theorem requires that a particle on the boundary remains on the boundary. Hence, for steady-state solutions

$$\mathbf{n} \cdot \mathbf{v}_{\text{particle}} = \mathbf{n} \cdot \mathbf{v}_{\text{boundary}}, \tag{2.6}$$

where $\mathbf{v}_{\text{particle}} = (u, v)_{\partial D}$ and $\mathbf{n}$ is the outward normal to the contour. For translating V-states (2.6) can be written as

$$u \sin \alpha - (v - V) \cos \alpha = 0, \qquad (x, y) \in \partial D_1 \quad \text{and} \quad \partial D_2, \tag{2.7T}$$

where V is the translational speed (the velocity is in the y-direction from Fig. 1a). For rotating V-states (2.6) can be written as

$$u \sin \alpha - v \cos \alpha = -\Omega R \frac{dR}{ds}, \qquad (x, y) \in \partial D, \tag{2.7R}$$

where Ω is the angular velocity of the state, s is the arclength, and $R(s)$ is the radius from the origin to the contour as shown in Fig. 1b. Note that for simplicity in (2.7) and henceforth we label equations with "T" (translating) or "R" (rotating) according to the state being considered. We now assume that the contours are "star-shaped," where the single-valued $R(\theta)$ is defined with respect to a convenient origin as shown in Fig. 1, so that

$$(x, y) = (R(\theta) \cos \theta + x_0, R(\theta) \sin \theta), \tag{2.8}$$

where

$$R(\theta) = |(x(\theta) - x_0)^2 + y^2(\theta)|^{1/2}$$

($x_0 = 0$ for the rotating case). Hence, (2.7) becomes

$$u dy/d\theta - (v - V) dx/d\theta = 0, \qquad (x, y) \in \partial D_1 \text{ or } \partial D_2, \tag{2.9T}$$

or

$$u dy/d\theta - v dx/d\theta + \Omega R \, dR/d\theta = 0, \qquad (x, y) \in \partial D. \tag{2.9R}$$

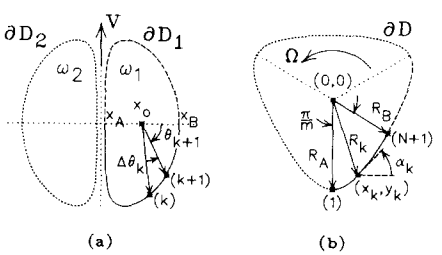

FIG. 1. Schematic and notation for V-states (the lines of symmetry are dotted). (a) Translating. Dipolar vorticity, $\omega_2 = -\omega_1$. (b) Rotating. The FAVR shown has 3-fold symmetry.

Also, we can use (2.8) to write (2.9) explicitly in terms of $R(\theta)$ as

$$dR/d\theta = \lambda R, \tag{2.10}$$

where

$$\lambda = |(V - v)\sin\theta - u\cos\theta|/|(V - v)\cos\theta + u\sin\theta| \tag{2.11T}$$

or

$$\lambda = -|u\cos\theta + v\sin\theta|/|u\sin\theta - v\cos\theta + \Omega R|. \tag{2.11R}$$

As discussed in Section 4 we will use (2.9) for our second-order scheme and (2.10) for our third-order scheme.

An alternative "stream function" form of the integral equations is obtained by writing (2.9) as

$$(\partial_y \psi)(dy/d\theta) + (V + \partial_x \psi)(dx/d\theta) = 0, \qquad (x, y) \in \partial D_1 \text{ or } \partial D_2, \tag{2.12T}$$

or

$$(\partial_y \psi)(dy/d\theta) + (\partial_x \psi)(dx/d\theta) + \Omega R\, dR/d\theta = 0, \qquad r = R(\theta), \quad (r, \theta) \in \partial D, \tag{2.12R}$$

and integrating to obtain

$$\psi(x, y) + Vx = c_j, \qquad (x, y) \in \partial D_j, j = 1 \text{ or } 2, \tag{2.13T}$$

or

$$\psi(r, \theta) + (\Omega/2)R^2(\theta) = c, \qquad r = R(\theta), \quad (r, \theta) \in \partial D. \tag{2.13R}$$

Pierrehumbert [8] used (2.13T) and Burbea and Landau [10] used (2.13R) to obtain steady-state solutions, whereas we use the "velocity" form as described above.

In this paper we solve two classes of problems:

Problem T (symmetric dipolar translating V-state): This state is symmetric about both axes as shown in Fig. 1a with vorticity $\omega_1 = +1$ and $\omega_2 = -1$. Then, given $x_B = 1$ and $0 \leqslant x_A \leqslant 1$ find $R(\theta)$ and V that satisfy (2.9T) or (2.10) with (2.11T).

Problem R (m-fold symmetric rotating V-state): This state with vorticity $+1$ has m identical sectors each of which has two reflectionally symmetric subsectors as shown in Fig. 1b for $m = 3$. Then, given m, $R_B \equiv R(\pi/m - \frac{1}{2}\pi) = 1$ and $R_A \equiv R(-\pi/2) > 1$ find $R(\theta)$ and Ω that satisfy (2.9R) or (2.10) with (2.11R).

3. Analysis for Limiting V-States

3.1. *Introduction*

In this section we summarize the local analysis of V-states, presented in detail elsewhere [15]. We use a local expansion to obtain the equation for the boundary of a symmetric dipolar translating or m-fold symmetric rotating V-state in the neighborhood of a *possible* singularity. The analysis provides a necessary condition for the behavior of the boundary. Namely, the *difference* in tangent angles at a singular point can be only $\pi/2$ (i.e., a corner) or, for the rotating case, 0 (i.e., the tangent angle is continuous but some higher derivative may be discontinuous). In Sections 3.2 and 3.3 we present this summary for the translating and rotating cases, respectively. In addition, in Section 3.4 the analysis is applied to Kirchoff's elliptical vortex to validate the procedure. In Sections 5 and 6, respectively, we compare this local expansion to the numerical results and obtain excellent agreement.

The general method of analysis is as follows. For convenience we use polar coordinates, (r, θ), with the singularity at the *origin*. As shown in Fig. 2 we assume that the V-state can be oriented so that it is symmetric about the y-axis and lies in the upper half plane (i.e., the vorticity on the negative y-axis is 0). We do all calculations in the right half-plane, i.e., $-\pi/2 \leqslant \theta \leqslant \pi/2$, using symmetry to complete the V-state. We assume in some neighborhood of the origin, $0 < r < \delta$, that the boundary, $\theta = \theta(r)$, is once continuously differentiable so that the tangent angle is continuous. (However, this does not preclude $\lim_{r\to 0} d\theta(r)/dr = \pm\infty$.) We expand the integral expression for ψ in (2.2) in terms of r to $0(r^2 \log r)$. Since the V-state is stationary in the appropriate reference frame, the value of the stream function, ψ^s, is constant on its boundary and so, without loss of generality, $\psi^s(r, \theta(r)) = 0$ for $0 \leqslant r < \delta$. We write $\theta(r)$ as

$$\theta(r) = \theta_0 + \theta_1(r), \tag{3.1}$$

where θ_0 is the tangent angle of the (right half of the) V-state at the origin, i.e., $\lim_{r\to 0} \theta(r) = \theta_0$, and so

$$\lim_{r\to 0} \theta_1(r) = 0. \tag{3.2}$$

Since ψ^s, the solution of Poisson's equation, (2.1b), is once continuously differentiable in all of $\mathbb{R}^2$, we can expand it in a Taylor series with remainder, or

$$0 = \psi^s(r, \theta(r)) = \psi^s(r, \theta_0 + \theta_1(r)) = \psi^s(r, \theta_0) + \partial_\theta \psi^s(r, \sigma)\, \theta_1(r), \tag{3.3}$$

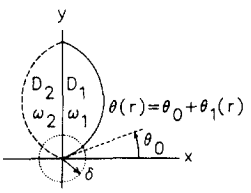

FIG. 2. Schematic and notation for a representative FAVR used in the analysis in Section 3. (Only in this section is the origin of the coordinate system at the singularity.)

where $\sigma \equiv \sigma(r)$ is in the *open* interval between θ_0 and $\theta_0 + \theta_1(r)$. Thus

$$\theta_1(r) = -\psi^s(r, \theta_0)/\partial_\theta \psi^s(r, \sigma(r)). \tag{3.4}$$

We obtain the possible value of θ_0 from (3.2), i.e.,

$$\lim_{r \to 0} \psi^s(r, \theta_0)/\partial_\theta \psi^s(r, \sigma(r)) = 0. \tag{3.5}$$

In those cases where $\psi^s(r, \theta_0) \not\equiv 0$, which includes the corner cases, we then expand ψ^s up to $0(r^2)$ and solve for $\theta_1(r)$ from (3.4). (To lowest order in r we can replace $\sigma(r)$ by θ_0.)

3.2. *Translating V-States*

The limiting symmetric translating V-state consists of two FAVRs with a common boundary on the y-axis and with vorticity $\omega_1 = +1$ and $\omega_2 = -1$. The right FAVR is composed of two contour segments, namely, $\theta(r)$ as described above and $\theta = \pi/2$, which is the common boundary. At the end of this subsection we will show that the two FAVRs of a limiting-case V-state cannot touch at only one point. (However, we cannot rule out the possibility of an *isolated* V-state whose FAVRs have one point in common.)

For $0 < \delta \ll 1$ and $r \ll \delta$, we find that [15]

$$\psi^s(r, \theta) = \left[V + \pi^{-1} \iint_{D_1} \cos \phi \, d\rho \, d\phi \right] r \cos \theta$$
$$- (4\pi)^{-1}(1 + \cos 2\theta_0) r^2 \log r \sin 2\theta + o(r^2 \log r), \tag{3.6}$$

where V is the speed of the V-state. Note that $\psi^s(r, \theta) = 0(r)$ if the leading term of (3.6) is nonzero. Thus, from (3.5) $\cot \theta_0 = 0$ so $\theta_0 = \pm\pi/2$. If the leading term vanishes, i.e.,

$$V = -\pi^{-1} \iint_{D_1} \cos \phi \, d\rho \, d\phi, \tag{3.7}$$

then (3.5) yields $\tan 2\theta_0 = 0$ so $\theta_0 = 0$ or $\pm\pi/2$. We first discuss $\theta_0 = 0$.

For $\theta_0 = 0$, from [15]

$$\psi^s(r, \theta) = -(2\pi)^{-1} r^2 \log r \sin 2\theta + (2\pi)^{-1}(C_1 + C_2) r^2 \sin 2\theta$$
$$- (4\pi)^{-1} r^2 \left[2\theta \cos 2\theta - \sin 2\theta + \begin{cases} \pi, & \text{if } \pi/2 \geqslant \theta > 0 \\ \pi \cos 2\theta, & \text{if } 0 > \theta \geqslant -\pi/2 \end{cases} \right]$$
$$+ o(r^2 \theta_1(r)), \tag{3.8}$$

where

$$C_1 = \iint_{D_1(\delta)} \rho^{-1} \sin 2\phi \, d\rho \, d\phi + (1/2)(1 + 2 \log \delta), \tag{3.9a}$$

$$C_2 = -\int_0^\delta \rho^{-1} \sin^2 \theta_1(\rho) \, d\rho, \tag{3.9b}$$

and $D_1(\delta)$ is that subset of D_1 whose distance from the origin is $>\delta$. From (3.4) we find that

$$\theta_1(r) = (\pi/4)/(-\log r + C_1 + C_2) + o((\log r)^{-2}). \tag{3.10}$$

Substituting (3.10) into (3.9b) we obtain a quadratic equation for C_2 and find that

$$C_2 = \tfrac{1}{2}[\log \delta - C_1 + ((\log \delta - C_1)^2 - (\pi^2/4))^{1/2}] + o((\log \delta)^{-2}). \tag{3.11}$$

The singular behavior of the curve near the origin, where $\theta_1(r) \ll 1$, can be seen from the slope,

$$\frac{dy}{dx} = \frac{\sin\theta(r) + r\cos\theta(r)\,\theta'(r)}{\cos\theta(r) - r\sin\theta(r)\,\theta'(r)} = \theta_1(r) + O(\theta_1^2(r)), \tag{3.12a}$$

and the curvature,

$$\begin{aligned}\kappa &= \frac{2\theta'(r) + r^2(\theta'(r))^3 + r\theta''(r)}{(1 + r^2(\theta'(r))^2)^{3/2}} \\ &= (8/\pi)\,\theta_1^2(r)/r + O(\theta_1^3(r)/r).\end{aligned} \tag{3.12b}$$

Note that the tangent angle is $O(1/\log r)$ and the curvature is $O(r^{-1}(\log r)^{-2})$ so that $\lim_{r\to 0}\kappa = \infty$. Also, the velocity at any point (r, θ) is

$$\begin{aligned} u &= -\pi^{-1} r \log r \cos\theta + \pi^{-1}(C_1 + C_2) r\cos\theta \\ &\quad - (2\pi)^{-1} r \left[-2\theta\sin\theta + \begin{cases} \pi\sin\theta, & \pi/2 \geqslant \theta > 0 \\ -\pi\sin\theta, & 0 > \theta \geqslant -\pi/2 \end{cases}\right] + o(r^2\,\theta_1(r)), \end{aligned} \tag{3.13a}$$

$$\begin{aligned} v &= -\pi^{-1} r \log r \sin\theta + \pi^{-1}(C_1 + C_2) r\sin\theta \\ &\quad - (2\pi)^{-1} r[2\theta\cos\theta + \pi\cos\theta] + o(r^2\theta_1(r)), \end{aligned} \tag{3.13b}$$

so that on the curve $u = O(r\log r)$ and $v = O(r)$.

For $\theta_0 = +\pi/2$, we show in [15] that

$$\psi^s(r, \theta) = C_0 r\cos\theta + (2\pi)^{-1} C_1 r^2 \sin 2\theta + o(r^2\cos\theta), \tag{3.14}$$

where

$$C_0 = V + \pi^{-1}\iint_{D_1} \cos\phi\, d\rho\, d\phi \tag{3.15a}$$

and

$$C_1 = \iint_{D_1} \rho^{-1}\sin 2\phi\, d\rho\, d\phi. \tag{3.15b}$$

Substituting $\theta = \theta_0 + \theta_1(r)$ in (3.14) we obtain

$$0 = \psi^s(r, \theta_0 + \theta_1(r)) = -C_0 r \sin \theta_1(r) - (2\pi)^{-1} C_1 r^2 \sin 2\theta_1(r) + o(r^2 \sin \theta_1(r)). \tag{3.16}$$

If we divide (3.16) by $r \sin \theta_1(r)$ and let $r \to 0$, we find that $C_0 = 0$. If we then divide (3.16) by $r^2 \sin \theta_1(r)$ and let $r \to 0$ we find that $C_1 = 0$. However, $C_1 = 0$ in (3.15b) if and only if the origin of the coordinate system is on the horizontal line through the centroid of D_1. That is, the two FAVRs *touch at only one point*. This follows because the integrand in (3.15b) is antisymmetric about $\phi = 0$ and the V-state is assumed to be symmetric about this horizontal line of symmetry of D_1. If we do the same analysis for $\theta_0 = -\pi/2$ we obtain the same result.

We now show that this configuration leads to a contradiction. If the analysis is repeated with the origin on this line of symmetry [15], then we again obtain (3.14) and so, again, $C_0 = 0$, which *contradicts* the value obtained from (3.15a). To see this we use the numerical solutions obtained in Section 5 (or in [8]). We estimate the integral in (3.15a) by taking the limit as $x_A \to 0$ of a circle of radius $(1 - x_A)/2$ centered at $((1 + x_A)/2, 0)$. From Fig. 4 this circle, which we denote by $C(x_A)$, lies inside the corresponding V-state, denoted by $D_1(x_A)$. Thus,

$$\iint_{D_1(x_A)} \cos \phi \, d\rho \, d\phi \geqslant \iint_{C(x_A)} \cos \phi \, d\rho \, d\phi = (\pi/2)(1 - x_A)^2/(1 + x_A), \tag{3.17}$$

and so

$$\pi^{-1} \iint_{D_1} \cos \phi \, d\rho \, d\phi \geqslant \frac{1}{2}. \tag{3.18}$$

From Table I, $0 > V \geqslant -0.258$ for all the V-states and so $C_0 > 0.2$. (Actually $C_0 \approx 0.6$ for $x_A = 10^{-7}$.) Thus, solutions with FAVRs touching at one point are excluded so the only possible solution is the corner solution shown in Fig. 3a.

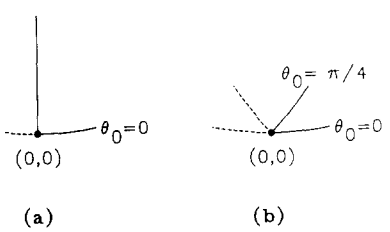

FIG. 3. Schematic showing the local behavior of the limiting V-state near the singularity at the origin. The possible values of θ_0 are described in Section 3. (a) Translating. The vertical line is the line of intersection of the two FAVRs. (b) Rotating.

TABLE I

Properties of the Translating V-States

Case	x_A	A	P	$\bar{x}$	V	V/V_0	$\bar{R}$	$\bar{R}/\bar{x}$	H	a
1	0.90	0.00786	0.314	0.950	−6.64E−4	1.000	0.0500	0.0527	0.0501	1.001
2	0.80	0.0316	0.631	0.900	−2.79E−3	1.000	0.100	0.111	0.101	1.006
3	0.70	0.0718	0.950	0.850	−6.72E−3	1.000	0.151	0.178	0.152	1.016
4	0.60	0.130	1.278	0.800	−0.0129	0.999	0.203	0.254	0.207	1.033
5	0.50	0.208	1.620	0.749	−0.0221	0.998	0.258	0.344	0.265	1.061
6	0.40	0.314	1.998	0.698	−0.0355	0.995	0.316	0.452	0.332	1.107
7	0.30	0.459	2.416	0.645	−0.0557	0.985	0.382	0.592	0.416	1.188
8	0.20	0.685	2.986	0.588	−0.0885	0.955	0.467	0.794	0.539	1.348
9	0.10	1.138	4.024	0.518	−0.149	0.852	0.602	1.162	0.786	1.747
10	0.05	1.597	5.071	0.474	−0.197	0.735	0.713	1.506	1.048	2.206
11	0.01	2.230	6.642	0.430	−0.245	0.593	0.843	1.959	1.451	2.932
12	1E−3	2.444	7.324	0.417	−0.257	0.550	0.882	2.116	1.629	3.262
13	1E−4	2.468	7.452	0.415	−0.258	0.545	0.886	2.135	1.662	3.325
14	1E−5	2.470	7.474	0.415	−0.258	0.544	0.887	2.137	1.668	3.335
15	5E−6	2.470	7.476	0.415	−0.258	0.544	0.887	2.137	1.668	3.336
16	1E−6	2.470	7.478	0.415	−0.258	0.544	0.887	2.137	1.668	3.337
17	1E−7	2.470	7.479	0.415	−0.258	0.544	0.887	2.137	1.669	3.337
Limiting	0	2.470	7.480	0.415	−0.258	0.544	0.887	2.137	1.669	3.338

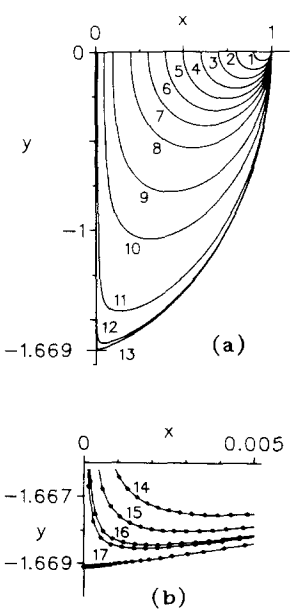

FIG. 4. (a) A sector of the translating V-states for cases 1 through 13 given in Table I. (b) A magnified view of the V-sates in the region of high curvature for cases 14 through 17 and the limiting case (the lowest curve). The dots are the nodes used in the numerical calculation.

3.3. *Rotating V-States*

For the rotating V-state we let $\omega_1 = \omega_2 = +1$ in Fig. 2 and find in [15]

$$\psi^s(r, \theta) = \left[\pi^{-1} \iint_{D_1} \sin \phi \, d\rho \, d\phi - \Omega \bar{y}\right] r \sin \theta + (4\pi)^{-1} \sin 2\theta_0 r^2 \log r \cos 2\theta + o(r^2 \log r), \tag{3.19}$$

where Ω is the angular speed of the V-state about the centroid at $(0, \bar{y})$. There are three cases to consider. First, if the leading term in (3.19) is nonzero then from (3.5) $\tan \theta_0 = 0$ so $\theta_0 = 0$. Second, if the leading term vanishes, i.e.,

$$\Omega = (\pi \bar{y})^{-1} \iint_{D_1} \sin \phi \, d\rho \, d\phi, \tag{3.20}$$

then (3.5) yields $\cot 2\theta_0 = 0$ so $\theta_0 = \pm \pi/4$. We will investigate only $\theta_0 = +\pi/4$, since the numerical results in Section 6 indicate that $\theta_0 = -\pi/4$ is not a limiting case. Third, if the leading term in (3.19) vanishes and $\theta_0 = \pi/2$ then (3.19) reduces to $\psi^{(s)}(r, \theta) = o(r^2 \log r)$ and (3.5) is not applicable (J. Burbea, private communication). However, we will show that we obtain a contradiction if we expand $\psi^{(s)}(r, \theta)$ to the next order in r for $\theta_0 = +\pi/2$. (Again, we do not consider $\theta_0 = -\pi/2$ since the numerical results in Section 6 indicate that it is not a solution.) The two possible solutions $\theta_0 = 0$ and $\pi/4$ are shown in Fig. 3b.

For case 1 where $\theta_0 = 0$ we find, from [15], that

$$\psi^s(r, \theta) = C_0 r \sin \theta + (2\pi)^{-1}(C_1 + C_2) r^2 \cos 2\theta - (1/4) r^2 \left[-2\Omega + \begin{cases} 1 - (1/2)\cos 2\theta, & \pi/2 \geqslant \theta > 0 \\ (1/2)\cos 2\theta, & 0 > \theta \geqslant -\pi/2 \end{cases}\right] + O(r^3), \tag{3.21}$$

where

$$C_0 = \pi^{-1} \iint_{D_1} \sin \phi \, d\rho \, d\phi - \Omega \bar{y}, \tag{3.22a}$$

$$C_1 = \iint_{D_1(\delta)} \rho^{-1} \cos 2\phi \, d\rho \, d\phi, \tag{3.22b}$$

and

$$C_2 = -(1/2) \int_0^{\delta} \rho^{-1} \sin 2\theta_1(\rho) \, d\rho. \tag{3.22c}$$

From (3.4) we obtain

$$\theta_1(r) = -(2C_0)^{-1}(C_1 + C_2 + \pi\Omega - (\pi/4)) r + O(r^2). \tag{3.23}$$

Substituting this into (3.22c) we obtain

$$C_2 = (2C_0)^{-1}(C_1 + \pi\Omega - \pi/4)\delta + O(\delta^2), \tag{3.24}$$

so

$$\theta_1(r) = -(2C_0)^{-1}(C_1 + \pi\Omega - \pi/4)(1 + (2C_0)^{-1}\delta)r + O(r\delta^2). \tag{3.25}$$

From Section 6 we find that for an analytical V-state $C_0 > 0$ and $C_0 \to 0$ as the limiting V-state is approached so that $\kappa \to \pm\infty$. At the limiting V-state the equation of the curve jumps to (3.30).

We will now show that if we let D_1 be the right half of the ellipse $(x/a)^2 + (y/b)^2 = 1$ we obtain the correct local solution. That is, if the equation for an ellipse in our coordinate system,

$$r = \frac{2\sin\theta}{b} \Big/ \left(\frac{\cos^2\theta}{a^2} + \frac{\sin^2\theta}{b^2}\right), \tag{3.26}$$

is expanded near the origin, the result, $r \approx 2a^2\theta/b$, agrees with (3.25). First we substitute (3.26) into (3.22a) and (3.22b) and obtain

$$C_0 = \pi b\left[\frac{a}{a+b} - \Omega\right], \tag{3.27a}$$

and

$$C_1 = \frac{1}{2}(b/a^2)\delta + \left(\frac{1}{2}\pi\right)\left[\frac{a-b}{a+b} - \frac{1}{2}\right] + O(\delta^2). \tag{3.27b}$$

For the ellipse $\Omega = ab/(a+b)^2$ [2] and if we substitute for Ω, C_0 and C_1 in (3.25), we obtain $\theta_1(r) = (\frac{1}{2}b/a^2)r + O(r\delta^2)$, which agrees with the expansion of (3.26) for $\theta \ll 1$. (Note that if $a = b$ then, for *arbitrary* Ω, $\theta_1(r) = \frac{1}{2}r/a + O(r\delta^2)$ as it should since the circular FAVR is a V-state for any Ω.)

For case 2 where $\theta_0 = \pi/4$, from [15]

$$\begin{aligned}\psi^s(r,\theta) = {} & (4\pi)^{-1}r^2 \log r \cos 2\theta + (2\pi)^{-1}(C_1 + C_2)r^2\cos 2\theta \\ & - (4\pi)^{-1}r^2\left[-2\pi\Omega + (1/2)\cos 2\theta + (\theta - \pi/2)\sin 2\theta \right. \\ & \left. + \begin{cases}\pi, & \text{if } \pi/2 \geqslant \theta > \pi/4 \\ \pi\sin 2\theta, & \text{if } \pi/4 > \theta \geqslant -\pi/2\end{cases}\right] + o(r^2\theta_1(r)),\end{aligned} \tag{3.28}$$

where

$$C_1 = \iint_{D_1(\delta)} \rho^{-1}\cos 2\phi \, d\rho \, d\phi - (1/4)(1 + 2\log\delta), \tag{3.29a}$$

and

$$C_2 = \int_0^{\delta} \rho^{-1} \sin^2 \theta_1(\rho)\, d\rho. \tag{3.29b}$$

Thus, from (3.4)

$$\theta_1(r) = [\Omega - (3/8)]\pi/(\log r + 2(C_1 + C_2)) + o((\log r)^{-2}). \tag{3.30}$$

Substituting (3.30) into (3.29) we obtain a quadratic equation for C_2 and find that

$$C_2 = -(1/4)|\log \delta + 2C_1 + ((\log \delta + 2C_1)^2 - 8\pi^2[\Omega - (3/8)]^2)^{1/2}| + o((\log \delta)^{-2}). \tag{3.31}$$

In this case the slope is

$$dy/dx = 1 + 2\theta_1(r) + O(\theta_1^2(r)), \tag{3.32}$$

while the curvature is

$$\kappa = -([\Omega - (3/8)]\pi)^{-1}\theta_1^2(r)/r + O(\theta_1^3(r)/r), \tag{3.33}$$

which is similar to the translating case, Eqs. (3.12). The velocity is also similar to that previously given.

For case 3 where $\theta_0 = \pi/2$, from [15]

$$\psi^s(r, \theta) = -(2\pi)^{-1}(C_1 + C_2)r^2 \cos 2\theta - (1/2)\,\Omega r^2 + o(r^2), \tag{3.34}$$

where

$$C_1 = \iint_{D_1(\delta)} \rho^{-1} \cos 2\phi\, d\rho\, d\phi \tag{3.35a}$$

and

$$C_2 = (1/2)\int_0^{\delta} \rho^{-1} \sin 2\theta_1(\rho)\, d\rho. \tag{3.35b}$$

Substituting $\theta = \theta_0 + \theta_1(r)$ into (3.34) we obtain

$$0 = \psi^s(r, \theta_0 + \theta_1(r)) = (2\pi)^{-1}(C_1 + C_2)r^2 \cos 2\theta_1(r) - (1/2)\,\Omega r^2 + o(r^2). \tag{3.36}$$

Dividing (3.36) by r^2 and letting $r \to 0$ we find that

$$\Omega = (C_1 + C_2)/\pi, \tag{3.37}$$

which we will now show is a contradiction since $\Omega > 0$ but $C_1, C_2 < 0$.

For a cusp $\theta_1(r) \leqslant 0$ and thus $C_2 < 0$ from (3.35b). The proof that $C_1 < 0$ relies on the fact that the integrand in (3.35a) is positive for $0 \leqslant \phi < \pi/4$ and negative for $\pi/4 < \phi \leqslant \pi/2$. For the proof, which is contained in [15], we find a domain $\mathscr{D}$ such that

$$C_1 < \iint_{\mathscr{D}} \rho^{-1} \cos 2\phi \, d\rho \, d\phi = 0. \tag{3.38}$$

We choose as our domain, $\mathscr{D}$, the square with vertices at $(0, 0)$, $(\bar{y}, 0)$, $(\bar{y}, \bar{y})$, and $(0, \bar{y})$. The positive part of the integral in (3.38), i.e., $0 \leqslant \phi \leqslant \pi/4$, is larger than the corresponding part of (3.35a). The negative part of the integral in (3.38), i.e., $\pi/4 \leqslant \phi \leqslant \pi/2$, is smaller in magnitude than that in (3.35a) since we are not including the subset of D_1 for which $y > \bar{y}$. Geometrically, it can be easily seen that $C_1 < 0$ for $m = 3$ and 4 from the limiting cases shown as the solid lines in Fig. 7 since the domain is entirely contained in $\pi/4 \leqslant \phi \leqslant \pi/2$.

3.5. *Summary*

In this section we have examined the behavior of a V-state in the neighborhood of a singularity. To apply the analysis we put the origin of the coordinate system at the point in question and then require that the V-state can be oriented to be symmetric about the y-axis as in Fig. 2. This can be done for both the symmetric dipolar translating V-state and the m-fold symmetric rotating V-state as shown in Figs. 4b and 7. (The analysis can also be done without assuming symmetry.) In the translating case we find that the *difference* in tangent angles at a singularity can be only $\pi/2$. We examine this corner case further and find that for $r \ll 1$ the curvature, κ, is $O(r^{-1}(\log r)^{-2})$, which indicates the difficulty in numerically calculating the V-state. In the rotating case we find that the *difference* in tangent angles at a singularity can be 0 or $\pi/2$. Again, for the corner case $\kappa = O(r^{-1}(\log r)^{-2})$. From numerical results 0 corresponds to an analytical V-state and $\pi/2$ to the limiting state for $3 \leqslant m \leqslant 6$ (and we assume for all $m \geqslant 3$). ($m = 2$ is a special case which does not have a limiting V-state—it approaches a vortex line with zero circulation, i.e., it vanishes.)

4. Numerical Algorithms

4.1. *Velocities*

We present new second- and third-order accurate algorithms. They both use a second-order accurate representation of the velocities on the contours $(u, v)_{\partial D}$, namely, a midpoint discretization of (2.5)

$$(u_k, v_k) = (2\pi)^{-1} \sum_{j=1}^{N_C} \omega_j \sum_{i=1}^{N_T^{(j)}} \frac{(x_k - \xi_{i-1/2}^{(j)}, y_k - \eta_{i+1/2}^{(j)})}{[(x_k - \xi_{i+1/2}^{(j)})^2 + (y_k - \eta_{i+1/2}^{(j)})^2]^{1/2}} (l_{k,i+1}^{(j)} - l_{k,i}^{(j)}), \tag{4.1}$$

where $(\xi_i^{(j)}, \eta_i^{(j)}) \in \partial D_j$, $N_T^{(j)}$ is the number of points on ∂D_j, and the mean positions are given by

$$f_{i+1/2} \equiv \tfrac{1}{2}(f_i + f_{i+1}) \tag{4.2}$$

and

$$l_{k,i}^{(j)} = [(x_k - \xi_i^{(j)})^2 + (y_k - \eta_i^{(j)})^2]^{1/2}.$$

4.2. *Second-Order Algorithm*

The second-order accurate algorithm is used to obtain translating V-states for $10^{-7} \leqslant x_A \leqslant 0.90$ and rotating m-fold symmetric V-states for

$$1.05 \leqslant R_A < R_A^*(m), \tag{4.3}$$

where $R_A^*(m)$ is the value at the corner. It converges more rapidly than the third-order iterative algorithm to be presented in the next subsection. However, for the limiting nonanalytical contours the third-order algorithm gives more accurate results as shown in Sections 5 and 6.

We use the second-order accurate discretization of (2.9),

$$u_{k+1/2}\,\Delta y_k - (v_{k+1/2} - V)\,\Delta x_k = 0, \qquad 1 \leqslant k \leqslant N, \tag{4.4T}$$

or

$$u_{k+1/2}\,\Delta y_k - v_{k+1/2}\,\Delta x + (\Omega/2)\,\Delta R_k^2 = 0, \qquad 1 \leqslant k \leqslant N, \tag{4.4R}$$

where $\Delta f_k \equiv f_{k+1} - f_k$ and $(u_{k+1/2}, v_{k+1/2})$ are defined in (4.2). Here, $N+1$ is the number of points on the segment of the contour for $-\pi/2 \leqslant \theta \leqslant 0$ in the translating case and $-\pi/2 \leqslant \theta \leqslant \pi/m - \frac{1}{2}\pi$ in the rotating case (the solid lines in Fig. 1). We define

$$(x_k - x_0,\, y_k) = R(\theta_k)(\cos\theta_k, \sin\theta_k), \tag{4.5}$$

where $x_0 = 0$ for the limiting translating V-state and all rotating V-states and $x_0 = \frac{1}{2}(x_A + x_B)$ for the analytical translating V-states. Substituting (4.5) into (4.4), we obtain

$$R_k - F_{k+1/2} R_{k+1} = 0, \qquad 1 \leqslant k \leqslant N, \tag{4.6a}$$

or, alternatively,

$$R_k - F_{k-1/2}^{-1} R_{k-1} = 0, \qquad 2 \leqslant k \leqslant N+1, \tag{4.6b}$$

where $F_{k+1/2}$ is defined as

$$F_{k+1/2} \equiv \frac{u_{k+1/2}\sin\theta_{k+1} - (v_{k+1/2} - V)\cos\theta_{k+1}}{u_{k+1/2}\sin\theta_k - (v_{k+1/2} - V)\cos\theta_k}, \tag{4.7T}$$

or

$$F_{k+1/2} \equiv \frac{u_{k+1/2}\sin\theta_{k+1} - v_{k+1/2}\cos\theta_{k+1} + (\Omega/2)R_{k+1}}{u_{k+1/2}\sin\theta_k - v_{k+1/2}\cos\theta_k + (\Omega/2)R_k}. \tag{4.7R}$$

To obtain convergent algorithms, we find it necessary to use a three-point scheme and a relaxation procedure. First we average (4.6a) and (4.6b) to obtain

$$-\tfrac{1}{2}F_{k-1/2}^{-1}\bar{R}_{k-1}+\bar{R}_k-\tfrac{1}{2}F_{k+1/2}\bar{R}_{k+1}=0, \qquad 2\leqslant k\leqslant N, \tag{4.8}$$

where $\bar{R}_1=R_A$ and $\bar{R}_{N+1}=R_B$. This discrete representation of our nonlinear integro-differential equation can be solved for R_k if we know $F_{k+1/2}$. Thus, if we have just completed the nth iteration we know $R_k^{(n)}$ and so can find $(u_{k+1/2}^{(n)}, v_{k+1/2}^{(n)})$ from (4.1). We then calculate the new velocity by summing (4.4) to obtain

$$V^{(n)}=\sum_{k=1}^{N}[u_{k+1/2}^{(n)}\,\Delta y_k^{(n)}-v_{k+1/2}^{(n)}\,\Delta x_k^{(n)}]/(x_A-x_B) \tag{4.9T}$$

or

$$\Omega^{(n)}=2\sum_{k=1}^{N}[u_{k+1/2}^{(n)}\,\Delta y_k-v_{k+1/2}^{(n)}\,\Delta x_k^{(n)}]/(R_A^2-R_B^2). \tag{4.9R}$$

Thus, we can calculate $F_{k+1/2}^{(n)}$ by (4.7) and solve the linear equation (4.8) for $\bar{R}_k\to\bar{R}_k^{(n+1)}$. We obtain $R_k^{(n+1)}$ by "relaxing" $R_k^{(n)}$ and $\bar{R}_k^{(n+1)}$ by

$$R_k^{(n+1)}=\mu^*\bar{R}_k^{(n+1)}+(1-\mu^*)R_k^{(n)}, \tag{4.10}$$

where $\mu^*=0.6$. We discuss the initial guess used in the appropriate section.

4.3. *Third-Order Algorithm*

Chronologically, we first obtained the second-order algorithm given in Section 4.2 but found that in the limiting cases it could give inadequate results. A third-order algorithm is readily obtained by using the differential equation for R, Eq. (2.10), and weighting three adjacent R_k in the manner described below. First, we discretize (2.11) using a midpoint method

$$\Delta R_k/\Delta\theta_k=\lambda_{k+1/2}R_{k+1/2}. \tag{4.11}$$

We rearrange and obtain

$$R_k-G_{k+1/2}R_{k+1}=0, \qquad 1\leqslant k\leqslant N, \tag{4.12a}$$

or

$$R_k-G_{k-1/2}^{-1}R_{k-1}=0, \qquad 2\leqslant k\leqslant N+1. \tag{4.12b}$$

Here $G_{k+1/2}$ is defined as

$$G_{k+1/2}\equiv(1-\tfrac{1}{2}\lambda_{k+1/2}\,\Delta\theta_k)/(1+\tfrac{1}{2}\lambda_{k+1/2}\,\Delta\theta_k), \tag{4.13a}$$

where

$$\lambda_{k+1/2}\equiv\lambda(u_{k+1/2}, v_{k+1/2}, R_{k+1/2}, (\sin\theta)_{k+1/2}, (\cos\theta)_{k+1/2}) \tag{4.13b}$$

and λ is defined in (2.11). The third-order property is achieved by weighting R_k in the following manner:

$$LR_k \equiv -\beta_k G_{k-1/2}^{-1} R_{k-1} + R_k - (1-\beta_k) G_{k+1/2} R_{k+1} = 0, \qquad 2 \leqslant k \leqslant N. \quad (4.14)$$

The local analysis, carried out in Appendix A, shows that terms $O((\Delta\theta_k)^3)$ cancel exactly if

$$-\beta_k(\Delta\theta_{k-1})^3 + (1-\beta_k)(\Delta\theta_k)^3 = 0. \quad (4.15)$$

(The algorithm discussed in Section 4.2 could be made third-order by the same type of procedure but it was easier to expand $G_{k+1/2}$, (4.13), rather than $F_{k+1/2}$, (4.7).)

In the translating case it was found that convergence could not be obtained for the limiting V-state, even for the third-order algorithm, when the boundary condition at the singularity was a fixed *angle* as opposed to a fixed *point*. (This is discussed further in Sections 5 and 6.) The solution oscillated over a small range in the neighborhood of the singularity.

Hence, to obtain convergence we use a two-step procedure: a method of stabilization [16] followed by a method of relaxation. For the method of stabilization we replace $LR_k = 0$ in (4.14) by a discretized version of $L\tilde{R}_k + \tilde{\mu}\partial_t \tilde{R}_k = 0$, where $\tilde{R}_k \to R_k$ as $t \to \infty$. That is, we solve for the $(n+1)$st iteration by

$$L(R_k^{(n)})\bar{R}_k^{(n+1)} + \mu(\bar{R}_k^{(n+1)} - R_k^{(n)}) = 0, \quad (4.16)$$

where we have introduced the intermediate variable $\bar{R}_k^{(n+1)}$ and $\mu = 0.1$. We again obtain $R_k^{(n+1)}$ by "relaxing" $R_k^{(n)}$ and $\bar{R}_k^{(n+1)}$ by (4.10). (Note that (4.10) and (4.16) are readily combined into one equation in our program.) If $\beta_k = \frac{1}{2}$ in (4.14) the algorithm is second-order accurate but not identical to the algorithm in Section 4.2. We have not used this second-order algorithm in this paper.

4.4. *Summary and Convergence Criteria*

The second- and third-order algorithms are summarized as follows:

(1) Compute $(u_{k+1/2}^{(n)}, v_{k+1/2}^{(n)})$ from $R_k^{(n)}$ using (4.1).

(2) Compute $V^{(n)}$ or $\Omega^{(n)}$ from (4.9).

(3) Compute $F_{k+1/2}^{(n)}$ from (4.7) or $G_{k+1/2}^{(n)}$ from (4.13) for the second- or third-order algorithms, respectively.

(4) Compute $R_k^{(n+1)}$ from (4.8) for the second-order algorithm or $\bar{R}_k^{(n+1)}$ from (4.16) and $R_k^{(n+1)}$ from (4.10) for the third-order algorithm. In either case use Gaussian elimination to invert the tridiagonal matrix.

(5) Continue the iteration until the error criterion is satisfied. A run is terminated if

$$\sum_{k=1}^{N+1} |R_k^{(n+1)} - R_k^{(n)}| < \varepsilon, \quad (4.17)$$

where

$$\varepsilon = \begin{cases} 5 \times 10^{-7} & \text{for translating states} \\ 5 \times 10^{-6} & \text{for rotating states.} \end{cases}$$

When convergence is obtained we find that the original integro-differential equations are satisfied to 5×10^{-8}, i.e.,

$$\max_k |u_{k+1/2}\, \Delta y_k - (v_{k+1/2} - V)\, \Delta x_k| < 5 \times 10^{-8}$$

or

$$\max_k |u_{k+1/2}\, \Delta y_k - v_{k+1/2}\, \Delta x_k + (\Omega/2)\, \Delta R_k^2| < 5 \times 10^{-8}.$$

This accuracy was verified on the DEC-10 (a 36-bit machine) at the University of Pittsburgh by continuing runs in double-precision once the required accuracy was obtained in single-precision.

5. Numerical Calculation of Translating V-States

5.1. *Analytical V-States*

To compute the sequence of states with $10^{-7} \leqslant x_A \leqslant 0.90$, we use the second-order algorithm. For case 1 the initial state is a half-circle of radius 0.05 centered at $(x_0, 0) = (0.95, 0)$, with $N+1$ equally spaced nodes, i.e., $\Delta\theta = \pi/N$. For the remaining cases in the sequence, the initial state is obtained by expanding linearly the previously obtained solution with $(x_0, 0) = (\frac{1}{2}(1 + x_A), 0)$. For cases 1–14, when the error, ε, (4.17), $\leqslant 10^{-4}$ we adjust the nodes so that the distance between the adjacent nodes is inversely proportional to the curvature, $R_{k+1/2}\, \Delta\theta_k \propto \kappa_{k+1/2}^{-1}$. This makes the local error the same in each interval [17]. For cases 15–17, $\Delta\theta_k$ is the same as obtained for case 14. With this discretization, we continue iterating until convergence is obtained.

The results obtained with the second-order algorithm and $N = 120$ are summarized in Figs. 4 and 5 and Table I. Figure 4a represents one sector, i.e., $\frac{1}{4}$ of the V-state, for

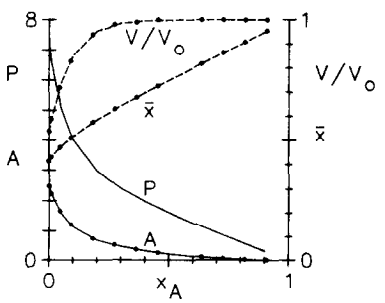

FIG. 5. Global properties for one contour of the translating V-state: A, area; P, perimeter; $\bar{x}$, x coordinate of the centroid; and, V/V_0, the normalized speed. The dots are the corresponding values from [8].

cases 1 ($x_A = 0.90$) through 13 ($x_A = 10^{-4}$). To show the power of the algorithm we have enlarged the scale by ≈400 in Fig. 4b and show cases 14 ($x_A = 10^{-5}$) through 17 ($x_A = 10^{-7}$). We observe that the contours are nested and tend to a limiting contour, the lowest in Fig. 4b, discussed below.

In Fig. 5 and Table I we present properties of the sequence of states where A is the area of one side, P is the perimeter, $\bar{x}$ is the x coordinate of the center of area, V is the translational speed, V/V_0 is the normalized translational speed, where $V_0 = A(4\pi\bar{x})^{-1}$ is the translational velocity of two point vertices with circulation $\pm A$ and separation $2\bar{x}$, $\bar{R} = (A/\pi)^{1/2}$, $H = \max|y|$ is the maximum vertical extent of a sector, and $a = 2H/(1 - x_A)$ is the aspect ratio. The dots in Fig. 5 are the results of Pierrehumbert [8] and the comparison is excellent except for H in the limiting case, as discussed below. The convergence criterion that $\varepsilon < 5 \times 10^{-7}$ is obtained with the second-order algorithm in less than 70 iterations. An iteration step with $N = 120$ requires 8 seconds of CPU on the DEC-10. Most of this time is consumed calculating the velocities at the nodes. A thorough discussion of accuracy and sensitivity is given in the following subsection.

5.2. *Limiting V-State* ($x_A = 0$)

As indicated in Fig. 4b the V-states tend to a limiting state. In Section 3 we observed that a limiting contour could approach the y-axis only when the tangent angle at the axis, α_1, is 0. In this subsection we investigate the sensitivity of this approach angle with the second- and third-order algorithms. The following paragraphs discuss the boundary conditions, initialization and discretization of this nonanalytical state.

We assume that the boundaries of both contours of the limiting V-state lie on the y-axis from $(0, -y^*)$ to $(0, y^*)$. We let the center of our polar coordinate system be at $(0, 0)$ and compute the velocities (u_k, v_k) in two parts. First, we do a numerical integration, Eq. (4.1), for $-\pi/2 \leqslant \theta \leqslant 0$ as previously and, second, we do an analytical integration of Eq. (2.4) from $(0, 0)$ to $(0, -y^*)$ as discussed in [1].

Two types of boundary conditions are used at $\theta = -\pi/2$. First, to find the corner solution we set $dy/dx|_{\theta=-\pi/2} = 0$ by fitting a quadratic polynomial, symmetric about the y-axis, through the second and third points. The resulting matrix can be transformed to a tridiagonal form and solved as previously. This limiting case is shown in Fig. 4b. We call this the *corner* boundary condition. Second, we fix the point on the y-axis, $R(-\pi/2)$, which enables us to determine the sensitivity of this limiting V-state.

Because of its singular character, as discussed in Seection 3, the limiting case is approached very slowly and the selection of a "good" initial state is important. As described in Appendix B the initial state is derived by smoothing the last analytical state (i.e., No. 17, $x_A = 10^{-7}$) with a high density of nodes near the corner as shown in Fig. 4b. We find, using the third-order algorithm and the corner boundary condition, that $y^* = 1.66855$, 1.66898 and 1.66911 for $N = 30$, 60 and 120, respectively. The convergence is very slow as the solution exhibits a damped oscillation around y^* and requires ≈3000 iterations to satisfy the error criterion. The second-

order algorithm solutions do not converge but simply oscillate slowly about y^* with a range of ≈ 0.001.

The calculations of y^* are consistent with the fact that the algorithm is actually only second-order accurate near the y-axis because (u, v) cannot be expanded in a Taylor series at the singularity (see (3.13)). Using second-order Richardson extrapolation on $N = 60$ and 120, we find to five significant figures

$$1.6691 \leqslant y^* \leqslant 1.6692. \tag{5.1}$$

Note that Pierrehumbert's limiting V-state has a cusp for the singularity and $y^* = 1.705$ $(=3.41/2)$. It seems to us that his distribution of nodes in the neighborhood of the singularity was inadequate since we could obtain "V-states" with $\alpha_1 = -\pi/2$ and $+\pi/2$ when the neighborhood of the singularity was inadequately resolved. (In Fig. 4b, $\Delta x_1 \approx 1.4 \times 10^{-5}$.)

In Fig. 6a we have plotted the limiting V-state in the neighborhood of the singularity for $N = 60$ and 120 (the dots). This is a magnification of ≈ 30 over Fig. 4b. Note that in Fig. 4b the tangent angle at $x = 0$ does not seem to be 0 (even with a magnification of ≈ 200) but is seen to be much closer to 0 in Fig. 6a (a magnification of ≈ 6000), which shows the singular nature of the curve.

Also in Fig. 6a we plot the equation for the curve (the solid line) from Section 3,

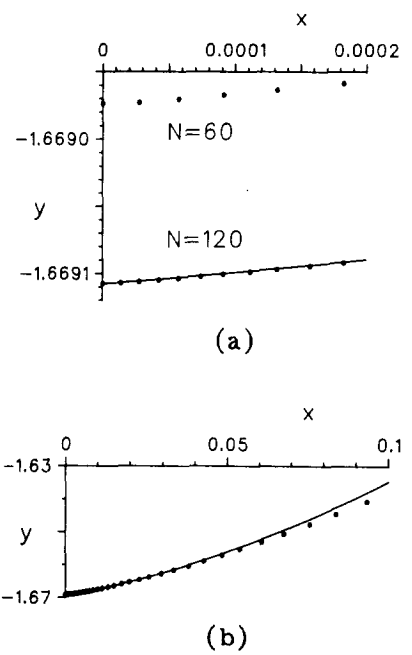

FIG. 6. A magnified view of the corner for the limiting translating V-state. (a) The dots are the numerical solutions obtained with the third-order algorithm and the corner boundary condition for $N = 60$ and 120. The solid line is the local solution, (3.10), fit to the $N = 120$ solution. (b) The comparison of Fig. 6a is on a larger scale.

TABLE II

The Limiting Translating V-State in the Neighborhood of the Corner ($N = 60$)

Algorithm	α_1	R_1	R_2	R_3	R_4	R_5
2nd	89.3°	1.665000	1.668862	1.668942	1.668963	1.668972
	37.6°	1.669001	1.669015	1.669012	1.669010	1.669006
	−0.8°	1.669015	1.669014	1.669012	1.669009	1.669005
	−13.2°	1.669021	1.669014	1.669012	1.669009	1.669005
	−89.7°	1.673000	1.669162	1.669069	1.669040	1.669023
3rd	89.7°	1.664974	1.668814	1.668894	1.668915	1.668924
	42.0°	1.668956	1.668973	1.668970	1.668967	1.668963
	−0.5°	1.668973	1.668972	1.668970	1.668967	1.668963
	−23.4°	1.668980	1.668972	1.668970	1.668967	1.668963
	−89.7°	1.673000	1.669162	1.669069	1.669040	1.669023

Eq. (3.10), with parameters C_1 and C_2 obtained from the solution with $N = 120$. C_1 has been calculated numerically from (3.9a) and C_2 from (3.11). For $\delta = 0.000014$, $C_1 + C_2 = 0.1196$, while even for $\delta = 0.049$, $C_1 + C_2 = 0.1106$. In Fig. 6b we continue this comparison on a larger scale to show the quality of the asymptotic formula. Also, the velocity of the V-state as calculated from (3.7) is −0.25797 while numerically it is −0.25793.

To determine the sensitivity of the algorithm we use the second boundary condition, i.e., fix $R(-\pi/2)$, near y^*. In Table II we show the results using both the second- and third-order algorithms for $N = 60$ where the x coordinates of the nodes correspond to those in Fig. 6a. Note that in all the cases the solution tends very rapidly to the corner solution. (We have given 7 significant figures for comparison purposes, but trust only the first 5.) For example, the maximum difference in R_1 is 1.673000 − 1.668973 = 0.004027 and in R_5 is 0.000060 (where $\alpha = -0.00013$). In all iterations.

6. Numerical Calculation of Rotating V-States

6.1 *Analytical V-States*

We compute the sequence of states for $1.05 \leqslant R_A < R_m^*$ with the second-order algorithm, where R_m^* is the value obtained for the limiting V-state. Our initial state is, for $-\pi/2 \leqslant \theta \leqslant \tilde{\theta}_m - \frac{1}{2}\pi$,

$$R^{(0)}(\theta) = R_A + (1 - R_A)\,\Theta(2 - \Theta), \tag{6.1}$$

where $\tilde{\theta}_m = \pi/m$, where $\Theta = (\theta + \frac{1}{2}\pi)/\tilde{\theta}_m$ and $\Delta\theta_k$ is constant. Fig. 7 shows (x, y) and curvature plots for one analytical V-state and the limiting V-state for $3 \leqslant m \leqslant 6$. In

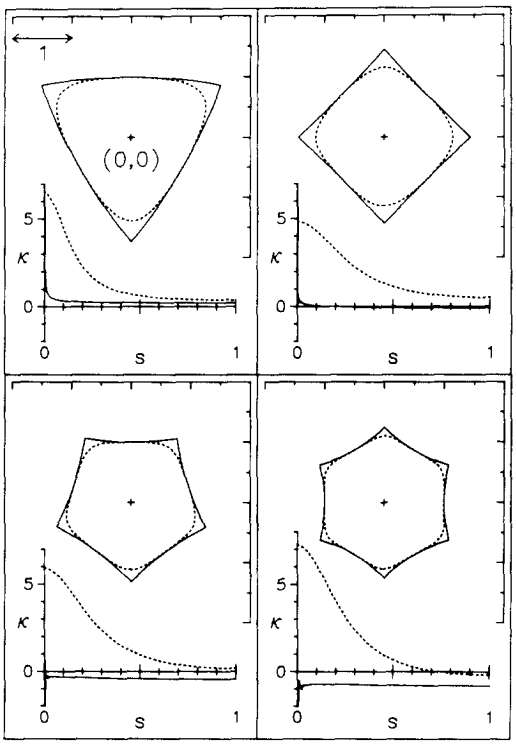

FIG. 7. Rotating V-states and their curvatures, $\kappa(s)$, for $3 \leqslant m \leqslant 6$. (The arclength is normalized so $s = 0$ at $\theta = -\frac{1}{2}\pi$ and $s = 1$ at $\pi/m - \frac{1}{2}\pi$.) The dashed curves are $R_A = 1.39256$ ($m = 3$), 1.14709 ($m = 4$), 1.11587 ($m = 5$) and 1.09855 ($m = 6$) in Table III. The solid curves are the limiting V-states.

the curvature plots the abscissa is the arclength scaled so that it is 0 at R_A and 1 at R_B. The properties of the analytical V-states are given in Table IIIa. The limiting cases (^{a}) are given for comparison and discussed below.

6.2. *Limiting V-State*

For the limiting V-state our initial state is

$$R^{(0)}(\theta) = R_A + (1 - R_A)\,\Theta^2(3 - 2\Theta), \tag{6.2}$$

where $R_A = 1.73$, 1.44, 1.32 and 1.24 for $m = 3$, 4, 5 and 6, respectively. The angular difference $\Delta\theta_k$ is either constant as in the analytical case or increases nearly linearly with k as discussed in Appendix B. For the latter we start with $\Delta\theta_1 = 0.1°$, 0.01° or 0.001°. We again use two types of boundary conditions at $\theta = -\pi/2$: the corner boundary condition, $dy/dx|_{\theta=-\pi/2} = +1$; and the fixed-point boundary condition, i.e., $R(-\pi/2) = R_A$. This corner boundary condition is obtained by using a linear combination of either the first 3 or 4 points, as described in Table IIIb.

Our results for $3 \leqslant m \leqslant 6$ are contained in Table IIIb for the corner boundary condition. Since the total number of points on the V-state is $2mN$ the time required

TABLE III

a. Properties of Rotating V-States

m	R_A	Ω	A	P	$1/R_A$
3	1.05000	0.33310	3.2967	6.4440	0.95238
	1.22128	0.32843	3.7967	7.0463	0.81881
	1.39256	0.31996	4.2382	7.7082	0.71810
	1.56384	0.30948	4.5909	8.4021	0.63945
	[a]1.73512	0.30122	4.7291	9.0652	0.57633
4	1.05000	0.37460	3.2947	6.4488	0.95238
	1.14709	0.37153	3.5684	6.8154	0.87177
	1.24418	0.36620	3.8046	7.2310	0.80374
	1.34127	0.35938	3.9870	7.6811	0.74556
	[a]1.43836	0.35395	4.0546	8.1380	0.69524
5	1.05000	0.39945	3.2927	6.4555	0.95238
	1.11598	0.39705	3.4726	6.7259	0.89616
	1.18174	0.39313	3.6263	7.0389	0.84621
	1.24761	0.38815	3.7426	7.3859	0.80153
	[a]1.31348	0.38425	3.7842	7.7534	0.76134
6	1.05000	0.41596	3.2909	6.4641	0.95238
	1.09855	0.41395	3.4193	6.6827	0.91029
	1.14711	0.41087	3.5284	6.9388	0.87176
	1.19566	0.40701	3.6097	7.2271	0.83636
	[a]1.24421	0.40407	3.6375	7.5415	0.80372

b. Properties of the Limiting Rotating V-States

m	N	Algorithm	BC	Discretization[b]	Ω_m^*	R_m^*	A	$1/R_m^*$
3	60	2nd	3	1° (C)	0.30126	1.7331	4.7273	0.57701
	60	2nd	3	0.1° (L)	0.30123	1.7349	4.7280	0.57640
	60	2nd	3	0.01 (L)	0.30122	1.7349	4.7281	0.57639
	60	3rd	4	0.01° (L)	0.30121	1.7353	4.7308	0.57626
	60	3rd	4	0.001° (L)	0.30117	1.7355	4.7337	0.57620
	120	2nd	3	[c] (L)	0.30124	1.7349	4.7283	0.57640
4	60	2nd	3	0.75° (C)	0.35392	1.4381	4.0541	0.69537
	60	2nd	3	0.01° (L)	0.35397	1.4383	4.0551	0.69528
5	60	2nd	3	0.6° (C)	0.38419	1.3137	3.7840	0.76123
	60	2nd	3	0.01° (L)	0.38429	1.3133	3.7842	0.76143
6	60	2nd	3	0.5° (C)	0.40399	1.2446	3.6376	0.80350
	60	2nd	3	0.01° (L)	0.40411	1.2441	3.6375	0.80382

[a] Designates the limiting cases as discussed in Section 6.2.

[b] C = Constant, L = "linearly" increasing.

[c] Corresponds to 0.01° with $N = 60$ and with an additional node midway between these nodes.

for each iteration increases as m^2 and so we will only consider the case $m = 3$ in detail. At the end we will comment about the other cases.

We perform a sensitivity study for $m = 3$ using various algorithms, boundary conditions and discretizations as shown in Table IIIb. With the "linearly" increasing discretization ($\Delta\theta_1 = 0.1°$, $0.01°$ and $0.001°$) we find

$$\begin{aligned} \Omega_3^* &= 0.30120 \pm 0.00004, \\ R_3^* &= 1.7352 \pm 0.0003. \end{aligned} \tag{6.3}$$

In the rotating case, unlike the translating case, both the second- and third-order algorithms converge to the limiting V-state for the corner boundary condition. The second-order algorithm converges in $\approx$500 iterations while the third-order algorithm requires $\approx$2000 iterations because the stabilization and relaxation procedures delay the convergence. Since the second-order algorithm is also much faster with the fixed-point boundary condition, we use only the third-order algorithm when high accuracy is required.

The range of existence of Ω_m for $2 \leqslant m \leqslant 6$ is shown as the solid vertical lines in Fig. 8 and Ω_m^*, the lower end of these lines, can be fit with

$$\tilde{\Omega}_m^* = \frac{1}{2}(m-2)\left[\frac{m - 1.195}{m^2 - 2.071m + .2085}\right], \tag{6.4}$$

where $|\tilde{\Omega}_m^* - \Omega_m^*| < 10^{-4}$. In previous analytical work [11] the lower end of the range of existence was given as $(1/2)(m-2)/(m-1)$, shows in Fig. 8 as the dots. This result is incorrect because Burbea *linearized* about the circular V-state and interpreted his results as being valid in the nonlinear region. In previous computational work [10] numerical solutions were obtained below our range of existence. For

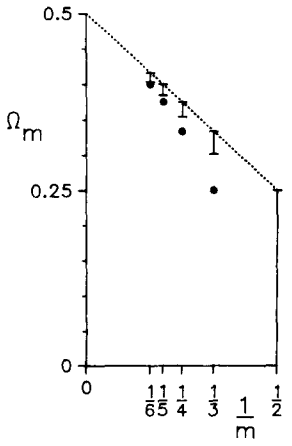

FIG. 8. Range of existence of rotating V-states for $2 \leqslant m \leqslant 6$. The dots are the lower end of the range from the incorrect analysis of Burbea [11].

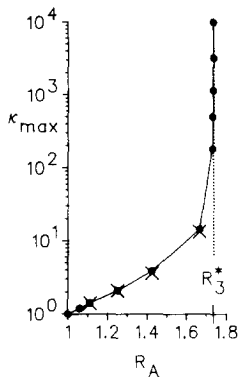

FIG. 9. Maximum curvature versus R_A for $m = 3$ rotating V-states. The dots correspond to the third-order algorithm (used with $\Delta\theta_1 = 0.01°$ for $R_A < 1.7$ and $0.001°$ for $R_A > 1.7$). The x's correspond to the results in [10].

example, for $m = 3$ they presented a solution at $\Omega = 0.2822$ which had regions of negative curvature. These incorrect results are probably due to inadequate discretization procedures and to the fact that spurious "solutions" can be obtained for $R_A > R_m^*$, as we will discuss below.

Since the range of existence of Ω_m was missed previously [10], we present the results of several sensitivity studies for $m = 3$ and R_A near R_3^*. First, the dots in Fig. 9 show the maximum curvature as a function of R_A obtained with the third-order algorithm, $N = 60$ and a discretization of $0.01°$ for $R_B < 1.70$ and $0.001°$ for $R_B > 1.70$. The x's are due to Burbea and Landau [10] and we have not plotted their last value of $\kappa = 236$ at $R_A = 1.923$, which is well to the right of the figure.

Second, we used the fixed-point boundary condition, both algorithms and various discretizations to obtain the results in Fig. 10a, where we have plotted the tangent angle at the singularity, i.e., α_1 vs R_A. The solid line shows the small range obtained for R_A, $1.735 \lesssim R_A \lesssim 1.736$, using the third-order algorithm and $0.01°$ ($0.001°$ is not shown since it is undistinguishable from $0.01°$). Also note that all solutions cross $\alpha_1 = 45°$ at $R_A \approx 1.735$. In Fig. 10b we show the behavior of the contours near R_3^* using the third-order algorithm and $0.001°$, where $R_A = 1.73333$, 1.73493 and 1.73559.

As shown in Fig. 10a, we can also obtain "solutions" for $R_A > R_3^*$ and, indeed, for $\alpha_1 \approx 90°$. This is due to the fact that the various discretized forms of Euler's equations have different solutions than the continuous equations, Eqs. (4.1). For larger values of R_A we still can obtain convergence, but we find that the solutions behave in a strange, algorithm-dependent, noncontinuous fashion. For example, for the third-order algorithm with $N = 60$ and $0.001°$ the solution jumps back from $\alpha_1 \approx 90°$ to $\alpha_1 \approx 0°$ as R_A is increased slightly (to ≈ 1.7358). For the remaining cases, $R(\theta_2)$ *decreases* as R_A increases until for $R_A = 1.80$ we find that $R(\theta_k) \approx 1$ $(= R_B)$ for $2 \leqslant k \leqslant N + 1$ so that the solution looks like a circle with a sharp spike. We take this

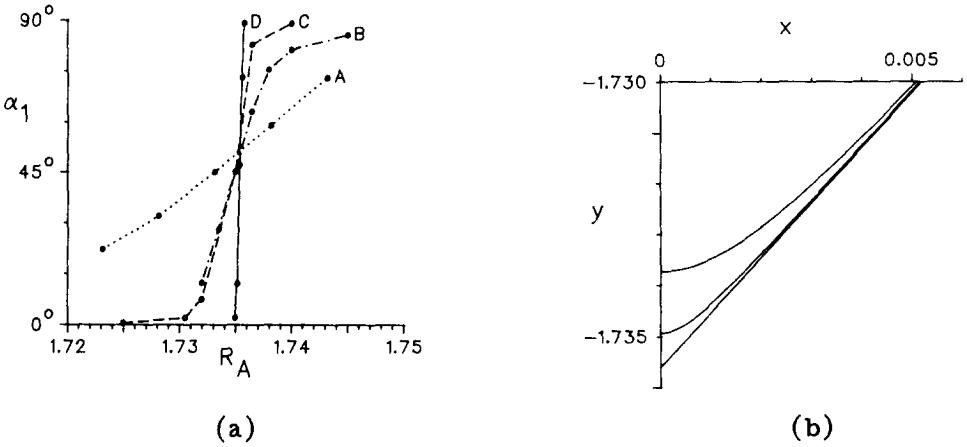

FIG. 10. A study of the behavior of the $m = 3$ rotating V-states near R_3^* using the fixed-point boundary condition. (a) α_1 is the tangent angle of the contour at $\theta = -\pi/2$. The algorithms and discretizations are: (A, dotted line) second order and 1° (constant); (B, dotted-dashed line) second order and 0.1° ("linearly" increasing); (C, dashed line) second order and 0.01° ("linearly" increasing); (D, solid line) third order and 0.01° ("linearly" increasing). (b) The behavior of selected contours near R_3^* for the third-order algorithm and 0.001° ("linearly" increasing).

as evidence that we have passed the range of existence of steady-state solutions to the continuum equations, which do not have V-states with cusps.

Finally, in Fig. 11 we compare the numerical results (the dots) for the 0.01° run with the 4-point boundary condition in Table IIIb to the formulas in Section 3, Eq. (3.30). C_1 has been calculated numerically from (3.29a) and then C_2 from (3.31). For $\delta = 0.00044$ then $C_1 + C_2 = -0.692$ while even for $\delta = 0.085$, $C_1 + C_2 = -0.694$. The comparison is excellent for the entire sector, $-\pi/2 \leqslant \theta \leqslant -\pi/6$. Also, Ω is 0.30122 from (3.20) while it is 0.30121 in Table IIIb. In Fig. 12 we compare an

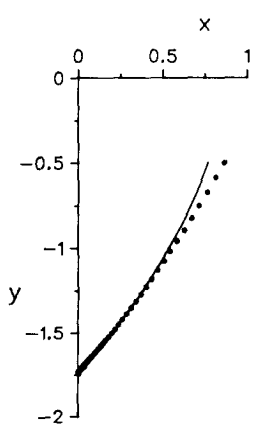

FIG. 11. A comparison of the limiting $m = 3$ rotating V-state for $-\pi/2 \leqslant \theta \leqslant -\pi/6$ using the third-order algorithm with 0.001° (the dots) and the analytical formula, Eq. (3.30).

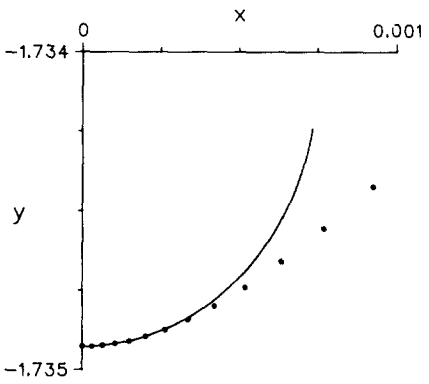

FIG. 12. A comparison of an analytical $m = 3$ rotating V-state, $R_A = 1.73493$ (the middle curve in Fig. 10b), with the analytical formula, Eq. (3.25).

[redacted] on the contour from the numerical calculation. Using the value of $s_2 = 0.501170$ we find that $C_0 = 0.00052$, $C_1 = -4.4489$ and the curvature at R_A obtained by differentiating (3.25) is $\kappa = 1495$, which agrees with the numerical solution to three significant digits. We consider all of the above a sufficient validation of our calculations of the limiting V-states.

The only difficulty we have encountered for $3 \leqslant m \leqslant 6$ is that the curvature oscillates near $\theta = -\pi/2$ as the limiting V-state is approached. In fact, the calculations of the V-states in Fig. 7 were done with the nodes equally spaced in angle (see Table IIIb) and for $m = 4, 5$ and 6 it is just possible to see wiggles in the curvature plots near the singularity (i.e., $s = 0$). (For $m = 3$ it is possible to remove the oscillations by a judicious choice of discretization while for $4 \leqslant m \leqslant 6$ the size and location of the oscillations change with the discretization but do not disappear.) However, for $3 \leqslant m \leqslant 6$, the curvature does have the correct sign *at* $\theta = -\pi/2$. That is, from (3.30) the curvature at R_A should be $+\infty$ for $m = 3$ and 4 since $(3/8) - \Omega > 0$, while it should be $-\infty$ for $m \geqslant 5$ since $(3/8) - \Omega < 0$. With sufficient nodes we believe these oscillations would disappear.

7. Discussion and Conclusions

We have presented new accurate (and fast) algorithms and refined procedures for computing symmetric translating and rotating V-states of the Euler equations in two dimensions. These include limiting *nonanalytical* contours with corner singularities that are compared with analytical solutions [15]. The agreement is excellent! These singularities were missed in previous numerical work [8, 10].

Burbea and Landau [10] proposed calling the rotating V-states "nonlinear Kelvin waves." However, "V-states" (vortex states) seems more appropriate since there are

already at least two types of Kelvin waves and since Deem and Zabusky first showed their existence [4] and coined the expression.

In all but the limiting cases the second-order accurate algorithm converges to the V-state quickly, both in the number of iterations (≈ 100) and the CPU time. The CPU time per iteration is $O(N^2)$ compared to Newton–Raphson, which is $O(N^3)$. The algorithms of Pierrehumbert [8] and Burbea and Landau [10] are also $O(N^2)$.

Our development of the third-order algorithm may seem ad hoc but came about in a search for an accurate method to calculate limiting V-states. We have used refined procedures to validate our results including various discretizations in the neighborhood of the singularity and two boundary conditions. In this paper we have not attempted to find procedures to minimize computation time. However, since most of the time in an iteration is taken up calculating the velocities, in recent work we have recalculated them every 20 iterations when $\varepsilon < 10^{-4}$. We find it reduces the computation time by a factor of 3.

We are presently using the new algorithms and have obtained asymmetric translating V-states and V-states with nested contours. The latter involves the solution of coupled integro-differential equations, one for each contour. However, there is a constraint that the velocities V or Ω for all contours must be equal.

Appendix A: Derivation of a Third-Order Algorithm

Since the velocities (u_k, v_k) are calculated by the trapezoidal rule (4.1), they are accurate to second order. Here, we show that we can obtain a third-order algorithm by properly weighting two equations.

Let $\hat{\lambda}$ and $\hat{R}$ be the solutions of $\hat{R}'(\theta) = \hat{\lambda}\hat{R}$, (2.10) (where primes denote differentiation with respect to θ), and $R_k \equiv R(\theta_k)$ be the solution of our self-consistent discrete representation (4.11). Let

$$\lambda_{k+1/2} = \hat{\lambda}_{k+1/2} + e_{k+1/2}, \tag{A.1}$$

where $e_{k+1/2} = O((\Delta\theta_k)^2)$. Then after some algebra (4.13) yields

$$G_{k+1/2} = \hat{G}_{k+1/2} \cdot (1 - e_{k+1/2}\,\Delta\theta_k) + O((\Delta\theta_k)^4), \tag{A.2}$$

where $\hat{G}_{k+1/2} \equiv G(\hat{\lambda}_{k+1/2})$. If we expand R_k in (4.12) about $\hat{R}_k$ we obtain

$$\hat{R}_k - \hat{G}_{k+1/2}\hat{R}_{k+1} = E_{k+1/2}(\Delta\theta_k)^3 + O((\Delta\theta_k)^4), \tag{A.3}$$

where

$$E(\theta) = (R'''/24) - (\lambda R''/8). \tag{A.4}$$

If we substitute (A.2) into (4.12a) and subtract (A.3) we obtain

$$\begin{aligned}(R_k - \hat{R}_k) - \hat{G}_{k+1/2}(R_{k+1} - \hat{R}_{k+1}) + e_{k+1/2}\,\Delta\theta_k \hat{G}_{k+1/2} R_{k+1} + E_{k+1/2}(\Delta\theta_k)^3 \\ = O((\Delta\theta_k)^4).\end{aligned} \tag{A.5}$$

We apply the same technique to (4.12b) and find

$$(R_k - \hat{R}_k) - \hat{G}_{k-1/2}(R_{k-1} - \hat{R}_{k-1}) - e_{k-1/2}\,\Delta\theta_{k-1}\,\hat{G}^{-1}_{k-1/2}R_{k-1} - E_{k-1/2}(\Delta\theta_{k-1})^3 = O((\Delta\theta_{k-1})^4). \tag{A.6}$$

To remove the leading order error, $O((\Delta\theta)^3)$, in (A.5) and (A.6), we multiply (A.5) by $1-\beta_k$ and (A.6) by β_k to obtain

$$\begin{aligned} &-\beta_k \hat{G}^{-1}_{k-1/2}(R_{k-1} - \hat{R}_{k-1}) + (R_k - \hat{R}_k) - (1-\beta_k)\,\hat{G}_{k+1/2}(R_{k+1} - \hat{R}_{k+1}) \\ &\quad + [\beta_k(-e_{k-1/2}\,\Delta\theta_{k-1}G^{-1}_{k-1/2}R_{k-1} + E_{k-1/2}(\Delta\theta_{k-1})^3) \\ &\quad + (1-\beta_k)(e_{k-1/2}\,\Delta\theta_k G_{k+1/2}R_{k+1} + E_{k+1/2}(\Delta\theta_k)^3)] = O((\Delta\theta)^4). \end{aligned} \tag{A.7}$$

Thus, we must choose β_k so that the term in brackets is $O((\Delta\theta)^4)$, namely,

$$-\beta_k(\Delta\theta_{k-1})^3 + (1-\beta_k)(\Delta\theta_k)^3 = 0. \tag{A.8}$$

This follows because, to lowest order, $\hat{G}^{-1}_{k-1/2} = \hat{G}_{k+1/2} = 1$, $R_{k-1} = R_{k+1}$, $E_{k-1/2} = E_{k+1/2}$, $e_{k-1/2} = c(\Delta\theta_{k-1})^2$ and $e_{k+1/2} = c(\Delta\theta_k)^2$ (for some c), where the latter three expressions are valid if the contour is analytic in the region from $k-1$ to $k+1$.

APPENDIX B: Initial Data and Distribution of the Nodes for Limiting Cases

B.1. *Translating Case*

In order to obtain the initial approximation $R^{(0)}(\theta)$ we begin with the nodes, $\{(x_k, y_k) \mid 1 \leqslant k \leqslant N+1\}$, from the 17th state, i.e., $x_A = 10^{-7}$. We find the value of k at which y_k is a maximum, say, $k = K$. Then we modify all (x_k, y_k) for $k \leqslant K+2$ by

$$x'_k = x_{K+3}|(k-1)/(K+2)|^{2.5}, \qquad 1 \leqslant k \leqslant K+2,$$

to obtain a nearly geometric ratio and

$$y'_k = P(x'_k), \qquad 1 \leqslant k \leqslant K+2,$$

where $P(x)$ is the unique quadratic function satisfying $y_{K+3} = P(x_{K+3})$, $y_{K+5} = P(x_{K+5})$ and $dP/dx|_{x=0} = 0$.

B.2. *Rotating Case*

The interval $-\pi/2 \leqslant \theta \leqslant \hat{\theta}_m - \pi/2$, where $\hat{\theta}_m = \pi/m$, is divided into $N+1$ angles by

$$\theta_k = -\pi/2 + \tilde{\theta}_m[(1+L)^{(k-1)/N} - 1]/L, \qquad 1 \leqslant k \leqslant N+1.$$

For $m = 3$ and $N = 60$ if $\Delta\theta_1 = 0.01°$ then $L = 691$, $\Delta\theta_N = 6.2°$ and the ratio of the largest $\Delta\theta$ to the smallest is ≈ 620. If $\Delta\theta_1 = 0.001°$, then $L = 9950$, $\Delta\theta_N = 8.5°$ and the ratio is ≈ 8500.

ACKNOWLEDGMENTS

This work was supported by the Army Research Office, Contract DAAG-29-80-K-0072, and the Office of Naval Research, Contract N00014-81-C-0531 (Task 062-583).

REFERENCES

1. N. J. ZABUSKY, M. H. HUGHES, AND K. V. ROBERTS, *J. Comput. Phys.* **30** (1979), 96.
2. H. LAMB, "Hydrodynamics," 6th ed., Section 159, p. 232, Dover, New York, 1932.
3. A. E. H. LOVE, *Proc. London Math. Soc.* (1) **25** (1893), 18.
4. G. S. DEEM AND N. J. ZABUSKY, *Phys. Rev. Lett.* **40** (1978), 859.
5. P. G. SAFFMAN AND R. SZETO, *Phys. Fluids* **23** (1980), 2339.
6. P. G. SAFFMAN AND R. SZETO, *Stud. Appl. Math.* **65** (1981), 223.
7. P. G. SAFFMAN AND J. C. SCHATZMAN, *SIAM J. Sci. Statist. Comput.* **2** (1981), 285.
8. R. T. PIERREHUMBERT, *J. Fluid Mech.* **99** (1980), 129.
9. R. T. PIERREHUMBERT AND S. E. WIDNALL, *J. Fluid Mech.* **102** (1981), 301.
10. J. BURBEA AND M. LANDAU, *J. Comput. Phys.* **45** (1982), 1.
11. J. BURBEA, *Lett. Math. Phys.* **6** (1982), 1.
12. R. G. SAFFMAN AND S. TANVEER, *Phys. Fluids* **25** (1982), 1929.
13. M. A. JASWON AND G. T. SYMM, "Integral Equation Methods in Potential Theory and Elastostatics," Academic, New York, 1977.
14. W. POGORZELSKI, "Integral Equations and Their Application," Vol. I, Pergamon, Elmsford, N.Y., 1966.
15. E. A. OVERMAN II, Steady state solutions of the Euler equations in two dimensions. II. Local analysis of limiting V-states, in preparation.
16. N. N. YANENKO, "The Method of Fractional Steps," Springer-Verlag, New York/Berlin, 1971.
17. N. J. ZABUSKY AND E. A. OVERMAN II, Regularization of contour dynamical algorithms. I. Tangential regularization, *J. Comput. Phys.* **52**, 351–373.